Semi-Automatic Vortex Extraction in 4D PC-MRI Cardiac Blood Flow Data using Line Predicates

Benjamin Köhler, Rocco Gasteiger, Uta Preim, Holger Theisel, Matthias Gutberlet and Bernhard Preim

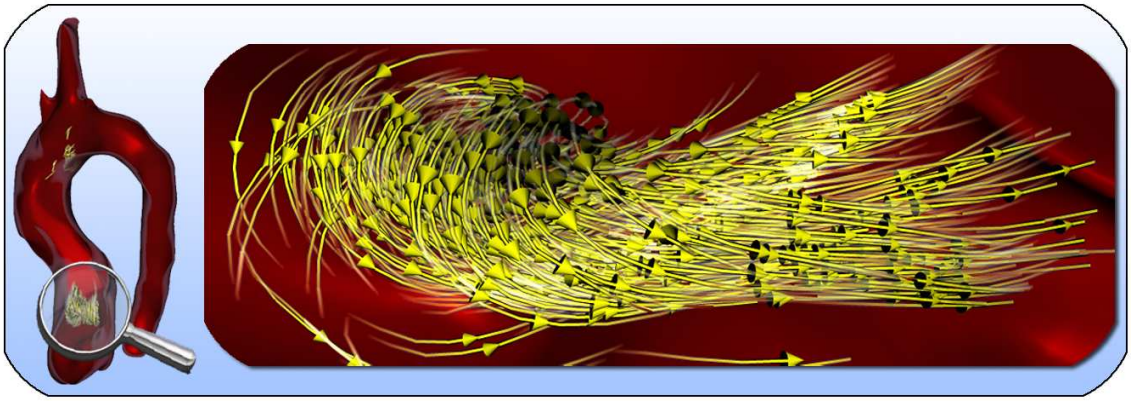

Fig. 1: *A diastolic vortex in the ascending aorta of a Tetralogy of Fallot patient is caused by retrograde flow into the left ventricle. This indicates an improperly closing aortic valve and supports the decision whether or not to implant an artificial valve.*

Abstract— Cardiovascular diseases (CVD) are the leading cause of death worldwide. Their initiation and evolution depends strongly on the blood flow characteristics. In recent years, advances in 4D PC-MRI acquisition enable reliable and time-resolved 3D flow measuring, which allows a qualitative and quantitative analysis of the patient-specific hemodynamics. Currently, medical researchers investigate the relation between characteristic flow patterns like vortices and different pathologies. The manual extraction and evaluation is tedious and requires expert knowledge. Standardized, (semi-)automatic and reliable techniques are necessary to make the analysis of 4D PC-MRI applicable for the clinical routine. In this work, we present an approach for the extraction of vortex flow in the aorta and pulmonary artery incorporating line predicates. We provide an extensive comparison of existent vortex extraction methods to determine the most suitable vortex criterion for cardiac blood flow and apply our approach to ten datasets with different pathologies like coarctations, Tetralogy of Fallot and aneurysms. For two cases we provide a detailed discussion how our results are capable to complement existent diagnosis information. To ensure real-time feedback for the domain experts we implement our method completely on the GPU.

Index Terms—4D PC-MRI, Cardiac Blood Flow, Hemodynamics, Line Predicates, Vortex Extraction

1 Introduction

As stated by the World Health Organization, cardiovascular diseases (CVD) are the leading cause of death worldwide [27]. Recent research shows the necessity to consider many different variables to judge a patient's situation. There is increasing evidence that in addition to the vessel morphology and wall motion, characteristic features of the blood flow are related to the severity of diseases and thus the urgency of treatment. With our work, we contribute to an improved diagnosis and treatment planning for conditions of the coronary vascular system like valve defects, congenital heart diseases and vascular dilations or narrowings.

Time-resolved and spatial phase-contrast magnetic resonance imaging (4D PC-MRI) is a non-invasive image modality that allows patient-specific flow measurements [24, 25]. The obtained hemodynamics can help to investigate the influence of pathological genesis, progression and outcome. The huge amount of data, however, makes the exploration and analysis a time-consuming, tedious and highly subjective task. The creation of standardized, (semi-)automated, and fast techniques for the emphasis of different data aspects and the extraction of anomalous flow characteristics like vortices was requested to answer specific questions and make 4D PC-MRI viable for the clinical routine [25]. Standardized methods do not only save time, but also decrease the inter-observer variability. While fully automatic approaches are not appropriate due to the large variety of anatomical situations and artifacts of the imaging process, a guided approach is described in this paper. Our focus is the detection of vortex flow in the human aorta and pulmonary artery, as vortices are a strong indicator for pathologies or for a higher risk for aneurysm development [4]. However, vortex patterns are not unique in a way that a certain shape reliably indicates one single pathology. Current research is more interested in the pure existence of vortex patterns in pathologic cases and correlations between pathologies and specific patterns. It is also about assessing the severity of pathologies and, thus, affects treatment choices [12].

The full entity of integral lines represents the spatio-temporal behavior of a flow field [4]. Thus, analyzing the characteristic of a vortex may be easier when integral lines that cover the whole swirling region are presented instead of vortex core lines. A common approach to get such integral lines is to extract vortex cores or regions in the flow

- *B. Köhler, R. Gasteiger, B. Preim and H. Theisel are with the department of Simulation and Graphics within the groups of Visualization and Visual Computing, University of Magdeburg, Germany. Email: {ben.koehler, gasteiger, preim}@isg.cs.uni-magdeburg.de, theisel@ovgu.de*
- *M. Gutberlet is head physician in the department of diagnostic and interventional radiology at the Herzzentrum in Leipzig, Germany. U. Preim is a radiologist and worked there for two years. Email: matthias.gutberlet@herzzentrum-leipzig.de, uta.preim@googlemail.com*

Manuscript received 31 March 2013; accepted 1 August 2013; posted online 13 October 2013; mailed on 27 September 2013.
For information on obtaining reprints of this article, please send e-mail to: tvcg@computer.org.

field and integrate lines in the close surrounding. To faithfully represent the unsteady cardiac flow, pathlines instead of streamlines are used [42]. Existing vortex core and region extraction techniques often deliver non-satisfactory results due to the noisy 4D PC-MRI data with low resolution. Consequently, the set of integrated pathlines will contain false-positive or false-negative findings and visual clutter. Our approach starts from the opposite point by calculating the full set of pathlines. Then, we embed local vortex criteria into the global line context using an adaption of the line predicates approach [4, 35, 38]. With a few processing steps, we extract pathlines representing the swirling regions in the flow. To the best of our knowledge, there is no work that compared different local vortex criteria and the reliability as well as quality of their results in the cardiac blood flow context. Thus, we focus on this gap and derive a recommendation. Cardiologists, radiologists and flow visualization experts served as advisors in all stages of the development. We put emphasis on maintaining the pathlines' quality. This refers to smooth, long, continuous and correct courses, which are easy to interpret. Our method provides reliable results and is easy to implement on the GPU.
Summarizing, the main contributions of this paper are:

- We perform a comparison of local vortex criteria in combination with line predicates and their suitability to extract vortices in 4D PC-MRI datasets of the aorta and pulmonary artery.
- We describe a semi-automatic and fast approach to extract expressive pathlines representing vortex regions.
- The evaluation with domain experts shows how clinically relevant information can be retrieved from the extracted flow characteristics. The relation between occurring vortices and different pathologies complements diagnosis information.

In Section 2, we give an overview of vortex extraction methods and their application to cardiac 4D PC-MRI datasets, current medical research about flow patterns in the aorta as well as pulmonary artery and the line predicate technique. Section 3 continues with details about cardiac pathologies, 4D PC-MRI data acquisition, arising challenges and our preprocessing pipeline. After discussing the requirements in Section 4, we proceed with the employed methods in Section 5. This includes an extension of the line predicates technique, the explanation of our vortex extraction procedure and the comparison of different local vortex criteria, followed by our recommendation. Afterwards, we apply the developed procedure to different pathologic cases in Section 6 and draw conclusions in Section 7.

2 Related Work

Medical Investigation of Flow Patterns: In biomedical research, the investigation of flow patterns and their relation to cardiovascular diseases (CVD) becomes an increased interest for both clinicians and biomedical engineers in recent years. Current research investigates correlations between certain characteristics like vortex shapes and orientations as well as flow complexity and stability to different pathologies. For instance, Hope et al. examine systolic flow patterns in the ascending aorta of patients with bicuspid aortic valves and manually classify vortices according to their orientation as right- and left-handed and according to their shape as helical and vortical flow. They define behaviors like nested flow that describes an inner right-handed vortex surrounded by an outer left-handed vortex or vice versa [15]. Francois et al. investigate right heart and pulmonary artery flow in Tetralogy of Fallot patients [8] and Bogren et al. tested the hypothesis that age and atherosclerotic coronary artery disease may influence aortic flow patterns [2]. Cebral et al. investigate the correlation between qualitative flow characteristics such as flow complexity and stability with respect to the risk of rupture for cerebral aneurysms [5]. Section 3.1 contains further details.

Visual Exploration: There are visual exploration approaches that help users to get insight into the patient's hemodynamics. For this purpose, a variety of tools is offered as well as expressive visualization techniques. Examples are illustrative techniques like speed lines by van Pelt et al. [43] and Born et. al [4], the FlowLens by Gasteiger et al. [9] and anatomy-guided exploration as well as map displays by Neugebauer et al. [28, 29]. Such methods are crucial in order to filter and emphasize important features and handle the vast amount of information.

Vortex Extraction: Furthermore, there are approaches that analyze the data by extracting features like vortices and critical points. Vortex extraction is an essential goal in the flow analysis. Existing methods can be divided into *local* and *global* approaches with lines representing vortex cores or regions with swirling behavior as a result. Local criteria are in many cases based on an analysis of the Jacobian matrix and fast to calculate, but may be sensitive to noise. Examples are the λ_2-criterion by Jeong and Hussain [19], the Q-criterion by Hunt [18], the reduced velocity by Sujudi and Haimes [40], cores of swirling particle motion by Weinkauf et al. [45], normalized helicity by Levy et al. [23], vorticity and torsion. Schafhitzel et al. state that the λ_2-criterion is most effective and most reliable [36]. Global algorithms return more precise results to the price of higher computation times. Further details are explained in Section 5.
Recent works applied some of those methods and extracted vortex cores in the aorta [39]. As expected, the results contain several false-positives due to the noisy data. Vortex cores were presented as spheres with their radius scaled proportionally to the swirling strength. To make the results easier to interpret, pathlines were calculated in the close surrounding of the vortex cores. Other real-world applications successfully employed the λ_2-criterion as well as reduced velocity and special seeding strategies to investigate the highly unsteady flow around dragonfly-wings [20].

Line Predicates: Line predicates, introduced by Salzbrunn et al. [35], provide an alternative approach to the flow field analysis. Several scalar criteria are computed for each point of an integral line and used for subsequent filtering. This approach does not only allow interval thresholding of the calculated values along an integral line, but also the combination of different criteria using set operations. Shi et al. provide a variety of suggestions for criteria [38]. Born et al. divide the computable measures into two categories, depending on the necessary data: line-based predicates like curvature solely consider the geometry of pathlines, whereas derived predicates like velocity and local vortex criteria utilize the underlying flow field [4]. They apply several predicates to extract different flow behaviors in 4D PC-MRI datasets of the aorta. Amongst others, they define a predicate to extract vortices. They use the approach by Sujudi and Haimes formulated with the parallel vectors operator by Peikert and Roth [31] to extract vortex core lines. Since the data are noisy, the results will include false-positives and a postprocessing step is inevitable. For this purpose, they use an ad hoc threshold of 30mm on the length of a vortex core line. A vortex is defined as detected, when a vortex core line is present and the condition from the λ_2-criterion is fulfilled in the corresponding voxel. Representative pathlines are then obtained by using a threshold on the Euclidean distance to the extracted vortex cores.

3 Medical Background

In the past years, 2D PC-MRI flow measurements were the common approach. A variety of quantitative measures are derived from single planes through the vessel. Their assessment plays a major role in rating the cardiac function and estimating the severity of pathologies. For instance, a low flow rate could denote cardiac insufficiency, retrograde flow in the diastole may indicate a valve defect and abnormal peak velocities hint at valve or vessel stenosis. The flow rate is calculated as integral of the length of velocity vectors projected onto the normal of a plane orthogonal to the vessel's centerline multiplied by the plane's area inside the vessel. Antegrade and retrograde flow is the integral of all positive and negative values, respectively.
Recent developments of 4D PC-MRI enable to obtain time-resolved 3D flow data. For an investigation of the hemodynamics, radiologists perform both a quantitative and qualitative analysis. For the quantitative analysis, planes orthogonal to the vessels centerline are usually employed. These planes can be freely moved and rotated, whereas the 2D method would require a whole new measurement. New challenges arise from the vastly increased data complexity. This particular

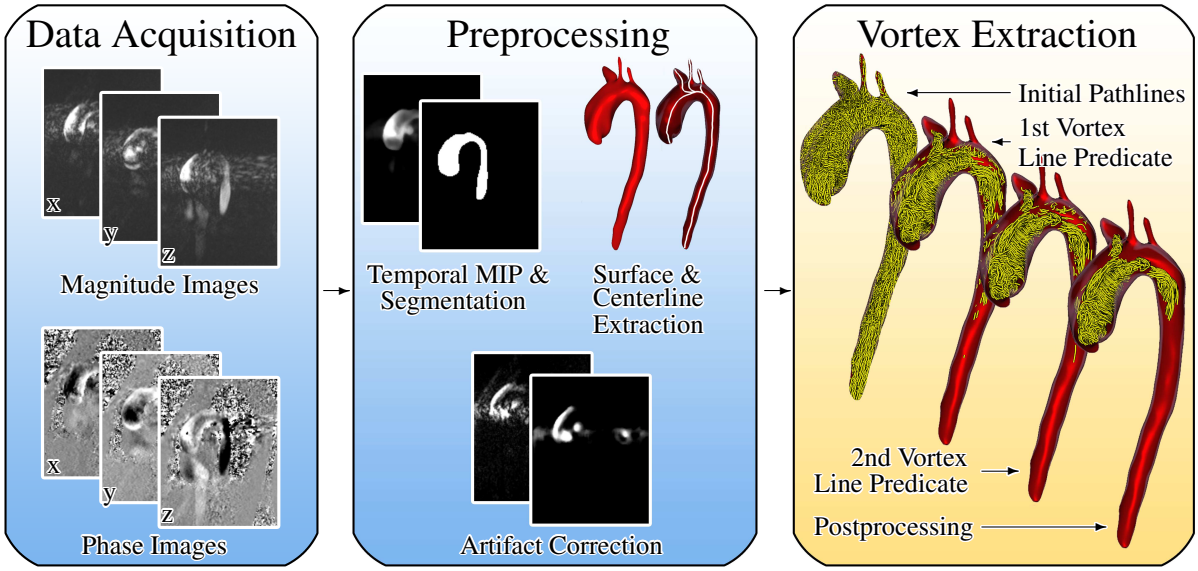

(a) (b) (c)

Fig. 2: *Preprocessing and vortex extraction pipeline. (a) The 4D PC-MRI flow measurement provides each three magnitude (top) and gradient images (bottom), which represent the x-, y- and z-direction and the strength of the flow, respectively. (b) We calculate a temporal maximum intensity projection (t-MIP) from the magnitude images, derive a segmentation and extract a triangular surface mesh with its centerline (top). Artifacts in the gradient images (eddy currents and phase wraps) are corrected (bottom). (c) Schematic illustration of our vortex extraction procedure using line predicates.*

kind of evaluation and diagnosis requires an advanced understanding of MR acquisition and interpretation of artifacts as well as in-depth knowledge of diseases and treatment options in cardiology. As a consequence, either radiologists with a focus on cardiac MRI and related diseases or cardiologists with a focus on imaging are involved and considered as domain experts for our work.
For the qualitative analysis, the depiction of certain flow characteristics like laminar or vortical flow is investigated. Typical visualization methods are streamlines for 3D as well as pathlines and particles for 4D data. A visualization of the entire flow leads to heavy visual cluttering and is challenging to interpret. Thus, emphasizing different flow data aspects and extracting various features like vortices is an indispensable step to convey the contained information appropriately.

3.1 Pathologies and Related Flow Behavior

There is a large number of highly diverse CVDs [27]. In the following, we explain selected pathologies, which are of main interest for 4D PC-MRI investigations, since they have altered vessel geometries in common that increase the probability of emerging vortex flow patterns.

Ectasias, Aneurysms and Coarctations: An ectasia names a local dilation of the aorta due to a weakened vessel wall. If the diameter is more than about 1.5 times the original size, it is called aneurysm. On the contrary, a coarctation denominates an abnormal narrowing of the aortic arch and can cause higher velocities due to the raised pressure. In both cases, the altered surface can enhance the formation of abnormal flow patterns like vortices.

Tetralogy of Fallot: The Tetralogy of Fallot is a complex congenital heart defect consisting of the following four components:

- A ventricular septal defect (VSD) causes a mixture of deoxygenated and oxygenated blood in the left ventricle. After a VSD surgery, which closes this hole in the cardiac septum and is the common treatment, patients have a high risk of developing an improperly closing pulmonary valve [13]. Increased vortex flow was observed in the right ventricle as well as the pulmonary artery in such cases compared to healthy volunteers. [8]
- Due to a stenosis in the pulmonary artery, the mixed blood from both ventricles is preferably pumped through the aorta. This behavior is called right-to-left shunt.
- A right ventricular hypertrophy develops progressively because of the constant resistance to blood flowing through the narrowed pulmonary artery.
- An overriding aorta names a special malposition, where the aorta is positioned directly over a VSD instead of the left ventricle.

Valve Defects: A bicuspid aortic valve (BAV) is the most common congenital aortic valve malformation. Normally, the aortic valve consists of three valvular leaflets, but in BAV patients two of them fused together. The aortic and pulmonary valves prevent blood from flowing back into the left and right ventricle during the diastole, respectively. BAVs are associated with nested helical flow and eccentric flow jets, which may help to identify patients' risk for ectasia development [1, 15].

Congestive Heart Failure: CHF is diagnosed when the heart is not able to provide enough blood to the body. Possible causes include a limited pump capacity or an abnormal amount of retrograde flow. The latter can occur during the diastole from the aorta back into the left ventricle or from the pulmonary artery back into the right ventricle, if the corresponding valve does not close properly. The percentage of retrograde flow is called regurgitation fraction. While a small amount up to 5% is considered as normal, higher percentages indicate CHF. Depending on the vessel with pathologic retrograde flow, aorta or pulmonary artery, it is termed aortic or pulmonary insufficiency.

Marfan Syndrome: The Marfan Syndrome is a genetic disorder of the connective tissue. Helical flow patterns in the ascending and descending aorta were significantly increased in Marfan patients compared to healthy subjects [11]. This could explain the susceptibility to ecastia development of such patients.

3.2 Data Acquisition and Preprocessing

Figure 2a shows the three magnitude and phase difference images obtained by a 4D PC-MRI acquisition. The former describe the strength of the flow for one temporal position and each phase image represents the component of the flow vectors in x-, y-, and z-direction, respectively. All temporal positions together represent one heart beat consisting of systole and diastole. Typical spatial resolutions are $150 \times 150 \times 50$ for 25 temporal positions with a voxel size of $2 \times 2 \times 2.5$mm [43].

However, measured blood flow data suffer from artifacts leading to an inaccuracy of the data. The artifacts comprise image noise, background distortions, and artifacts due to respiratory movements. Moreover, 4D PC-MRI data acquisition requires setting a velocity encoding parameter (VENC) that limits the maximum measurable velocity per direction. The outcome of choosing a too high VENC value is that low velocity values are less reliably measured. On the contrary, if the velocity exceeds the chosen VENC, the value will flip to the other end of the domain – called phase wrap. Thus, a preprocessing is necessary to correct the acquired datasets. It is likely that not all artifacts are completely removed. As a consequence, high demands in terms of robustness are placed upon algorithms dealing with 4D PC-MRI data. For our work, we use ten datasets acquired at a university hospital specialized in heart surgery, cardiology and pediatric cardiology. Besides two healthy volunteers, our datasets contain the following pathologies: two ectasias in the ascending aorta, one coarctation, one coarctation with a dilated ascending aorta, one bypass, one former coarctation with an aneurysm in the subclavian artery and an ectasia in the distal aortic arch, one Tetralogy of Fallot after VSD surgery and one coarctation treated with a prosthesis.

Aquisition: For the acquisition a 3 Tesla Siemens Verio MR scanner was used. The VENC was set to 1.5m/s in all acquisitions – an often used standard value in this context. The obtained spatial resolution is 1.77mm^2 in a 132×192 grid inplane with a distance of 3.5mm for each of the 15 to 23 slices. The temporal resolution varies from 14 to 21 time steps with about 50ms difference between each time step.

Preprocessing: To reduce the artifacts, the phase images were preprocessed using an eddy current correction [22] and a phase unwrapping [6] provided by the MeVisFlow software [14], shown in the bottom part of Figure 2b. The upper part illustrates a maximum intensity projection of the magnitude images over time (temporal MIP) that we used to obtain a binary segmentation mask. It serves as a flow mask and as input for the surface extraction via marching cubes. The meshes were reduced using quadric decimation by Hoppe et al. [16] and smoothed using a low-pass filter [41]. Figure 2c schematically shows the procedure of our later described vortex extraction.

4 Requirement Analysis

The majority of vortex extraction methods is designed for 3D steady flow fields, whereas methods for 3D unsteady flow like cores of swirling particle motion are rare [45]. Although the vortex cores of streamlines and pathlines can be similar when the flow changes only slightly, there is no guarantee that they match.
The identification of the most suitable local vortex criterion in combination with line predicates requires an extensive evaluation. Considered aspects are mainly not precise enough to put them into a mathematical description and, since there is no ground truth, we have to rely on subjective evaluations of domain experts.
To make the characteristics of a vortex easy to interpret, it is necessary to preserve pathlines of high quality. Thus, we have to avoid their fragmentation during the filtering process and instead maintain continuous and smooth courses. In order to achieve the desired high computational performances, the GPU's potential has to be utilized.
Summarizing, our discussion with domain experts suggests to focus on the following requirements:

- Find the local vortex criterion that provides the best results combined with our extraction procedure.
- Assess the suitability of 3D vortex criteria applied to the 4D blood flow.
- Ensure independent calculations to make our approach easy to implement on the GPU.
- Maintain easy to interpret high-quality pathlines during the subsequent filtering.
- Be able to derive clinically relevant information from the results provided by our approach.

5 Comparison of Vortex Criteria and Extraction Procedure

In this section, we discuss the extraction of vortices in measured 4D PC-MRI datasets of the aorta and pulmonary artery using line predicates. We shortly recall the line predicate technique and present our extension. Then, we describe the generic vortex extraction scheme, where different vortex criteria with particular thresholds are employed. This is followed by comparing the results achieved with different vortex criteria in collaboration with domain experts. Thereby, we define key questions to enable a qualitative comparison.

5.1 Extension of Line Predicates

The definition by Salzbrunn et al. [35] describes a line predicate P as a Boolean function mapping a point p of a pathline $\mathbb{P}$ to *true* or *false*:

$$\begin{aligned} P : \mathbb{P} &\rightarrow \{\mathit{true}, \mathit{false}\} \\ p &\mapsto P(p) \end{aligned} \tag{1}$$

To every point p a value $\hat{p}$ is assigned. A predicate filters all points that do not lie within a certain interval. All remaining points that are mapped to *true*, are called the characteristic set $\mathbb{C}_P$:

$$\mathbb{C}_P = \{(\vec{x},t) \in D \times I \mid P(p_{\vec{x},t}) = \mathit{true}\},\ \vec{x} \in D,\ t \in I \tag{2}$$

D is the $\mathbb{R}^3$ domain of the flow field and I is the set of all temporal positions. The common set operations like union and difference provide the possibility to connect different characteristic sets and combine multiple line predicates.
Born et al. [4] suggested a classification of line predicates according to the necessary data for the calculation: line-based predicates depend solely on the pathlines' geometry and derived predicates use the underlying flow field. We rename these two classes as geometry and flow field predicates, P_Γ and $P_\mathbb{V}$, respectively, and propose three further groups:

- Mesh predicates P_M utilize the explicit vessel representation. An example is the minimal distance of a point to the surface.
- Stream predicates P_Ω depend on surrounding pathlines. For instance, the number of pathlines weighted by their distance to each other can be used as a density value.
- To modify the values of one integral line in different ways, we created meta predicates P_{meta} as a superclass:
  - The sum predicate P_Σ adds up all calculated values $\hat{p}_i$ along an integral line weighted by the corresponding segment lengths $L(\cdot)$ and assigns this value to each of the N points:

$$P_\Sigma = \frac{\sum_{i=0}^{N-1} \left(\hat{p}_i \cdot \mathrm{L}(p_i)\right)}{\sum_{k=0}^{N-1} \mathrm{L}(p_k)} \tag{3}$$

    By applying this meta predicate, longer pathlines implicitly score higher than shorter ones.

  - The mean predicate $P_\oslash$ assigns the average value to each point. It is calculated as the sum predicate divided by N.

  - The smoothing predicate $P_{\sigma,n}$ applies a one-dimensional binomial filter with a kernel size of 3 in n iterations to the values along an integral line.

We use a simplified notation to describe the application of a series of line predicates to all existing pathlines. A characteristic set results in:

$$\mathbb{C}_P = P_1,\ t_1 \ \rightarrow\ P_2,\ t_2 \ \rightarrow\ \ldots \ \rightarrow\ P_n,\ t_n \tag{4}$$

where P_i is the subsequently applied line predicate with the corresponding thresholds t_i. A threshold can be one of the following:

- $\hat{p} \lessgtr v$: all values below or above v are valid.

- $v_0 \leq \hat{p} \leq v_1$: all values between v_0 and v_1 are valid.
- $\overline{v\%} = \hat{p} \geq \hat{p}_{\min} + \frac{v}{100} \cdot (\hat{p}_{\max} - \hat{p}_{\min})$: the upper $v\%$ of the values are valid.
- $\underline{v\%} = \hat{p} \leq \hat{p}_{\min} + \frac{v}{100} \cdot (\hat{p}_{\max} - \hat{p}_{\min})$: the lower $v\%$ of the values are valid. (5)

The application of a meta predicate is denoted as $P_{\text{meta}}(P)$, where $P_{\text{meta}} \in \{P_{\sum}, P_{\oslash}, P_{\sigma,n}\}$ and $P \in \{P_{\mathbb{V}}, P_{\Gamma}, P_M, P_{\Omega}\}$.
The following characteristic set is an example for a better understanding of the procedure:

$$\begin{aligned} \mathbb{C}_P = \quad & P_{\sigma,n}(P_{\mathbb{V}}^{\text{velocity}}),\ \overline{v_0\%} \\ \rightarrow \quad & P_{\Gamma}^{\text{length}},\ \hat{p} \geq v_1\ mm \end{aligned} \tag{6}$$

After the first step, $\mathbb{C}_P$ contains all points that represent the upper $v_0\%$ of the velocity domain after applying a smoothing predicate with n iterations. From this result, all pathlines shorter than v_1 mm are removed in the second step.

5.2 Pathline Integration and Vortex Extraction

Initialization: We start our procedure by covering the whole dataset inside the segmentation mask with pathlines started at spatially and temporally uniformly distributed seed positions. The necessary amount of pathlines depends on the data resolution and the flow field's changes over time. In our cases, $25,000 - 35,000$ pathlines were sufficient to produce results with the desired density. More sophisticated approaches could be applied at this point [32].

Vector Interpolation and Pathline Integration: Pathlines are integrated entirely on the GPU using an adaptive stepsize Runge-Kutta-4 method [7]. A vector $\vec{v} \in \mathbb{R}^3$ in the 3D flow field $\mathbb{V}_t$ of one temporal position t is obtained by hardware-accelerated trilinear interpolation. To interpolate a vector at the spatio-temporal position $\vec{x} = (x, y, z, t)$, the two neighboring temporal positions t_0 and t_1 are determined. The vectors $\vec{v}_{t_0}$ and $\vec{v}_{t_1}$ are calculated in the corresponding flow fields $\mathbb{V}_{t_0}$ and $\mathbb{V}_{t_1}$. Afterwards, $\vec{v}_{t_0}$ and $\vec{v}_{t_1}$ are interpolated linearly, weighted by the inverse temporal distances $1 - \| t - t_0 \|$ and $1 - \| t - t_1 \|$. In other words, we apply quadrilinear interpolation by using the GPU's fast trilinear interpolation twice and doing the last linear interpolation manually. Because of the rather small dataset resolutions we are able to store all flow fields of all temporal positions in the GPU's memory at once. Larger datasets would make an asynchronous data streaming necessary like shown by Venkataraman [44].

Jacobian Matrix Estimation: Local vortex criteria are in many cases based on an analysis of the Jacobian matrix or a derived matrix based on the Jacobian. So, its robust estimation increases the chance for proper results considerably. The calculation of one single Jacobian matrix for a whole voxel will deliver discontinuities at the voxel boundaries and affect the quality of the results negatively. Instead, we use central differences of the interpolated vectors $\vec{v} \in \mathbb{R}^3$ at the exact query positions $\vec{x} \in \mathbb{R}^4$ and the displacements $\pm\Delta\{x, y, z\}$. The offset in each direction is set to one corresponding voxel dimension and decreased successively if one of the shifted positions is not within the segmentation mask. We stick to central differences even near the segmentation mask boundaries, because we assume that they ensure better results than forward and backward differences. The multiple vector interpolations enable the smooth capturing of changes of the Jacobian matrix.

Line Predicate 1 - Finding Vortices: To extract vortex structures via line predicates, we use the following procedure.
First, we calculate a local vortex criterion as flow field predicate $P_{\mathbb{V}}^{\text{vortex}}$. Since the result tends to be noisy, a smoothing predicate $P_{\sigma,25}$ is applied before thresholding: $P_{\sigma,25}(P_{\mathbb{V}}^{\text{vortex}}),\ t_0^{\text{vortex}}$. On the one hand, line segments with values that indicate swirling behavior are extended. Consequently, longer segments remain after applying the threshold. On the other hand, outliers, i.e. single values indicating non-swirling-regions within a segment of swirling-values, diminish. Hence, thresholding does not interrupt the corresponding segments. As a result, the average filtered pathline length increases. However, the application of a smoothing predicate does not solve but at least reduce the fragmentation problem. We recommend to choose a very low threshold, just enough to crop certain non-swirling parts of the pathlines. Figure 3a shows a comparison without (top) and with (bottom) the application of a smoothing predicate. The noise reduction and increased average pathline length is especially noticeable in the right vortex in the distal aortic arch in this example. Due to the local nature of the vortex criteria, they can easily be calculated in parallel on the GPU.

Line Predicate 2 - Refining the Vortex Shapes: Sum and mean predicates apply the same value to every point of a pathline. As a consequence, pathlines can be removed or kept as a whole when thresholding, but further fragmentation is impossible. Therefore, we continue by applying a mean predicate of our local vortex criterion: $P_{\oslash}(P_{\mathbb{V}}^{\text{vortex}}),\ t_1^{\text{vortex}}$.

Line Predicate 3 - Postprocessing: Despite the application of the smoothing predicate it is likely that some short pathline fragments will occur, which decrease the visual quality. Thus, an additional postprocessing step is applied to remove these fragments properly. We employ a bending energy predicate, which is the sum predicate of curvature values: $P_{\Gamma}^{\text{bendingEnergy}},\ t_2 = P_{\sum}(P_{\Gamma}^{\text{curvature}}),\ t_2$. Based on this measure, a subsequent thresholding preserves long curved pathlines. Figure 3b shows the comparison of a result without (top) and with (bottom) the application of a bending energy predicate for postprocessing.

Visualization: The results are presented using standard techniques like illuminated streamlines, halos [26], particles with trails [43] enclosed by a ghosted view approach of the vessel surface [10]. Of course, other techniques like illustrative stream surfaces [3, 17] are also applicable. Color-coding by velocity is de-facto a standard in radiology. Mapping other attributes like directions to color can be highly misleading for physicians according to our experiences. Since velocities are not relevant for our work, we decided to employ uniformly colored pathlines to avoid distractions.
In the following, we will investigate which vortex criterion $P_{\mathbb{V}}^{\text{vortex}}$ provides the best results. Afterwards, we suggest reasonable thresholds for the placeholders t_0^{vortex}, t_1^{vortex} and t_2.

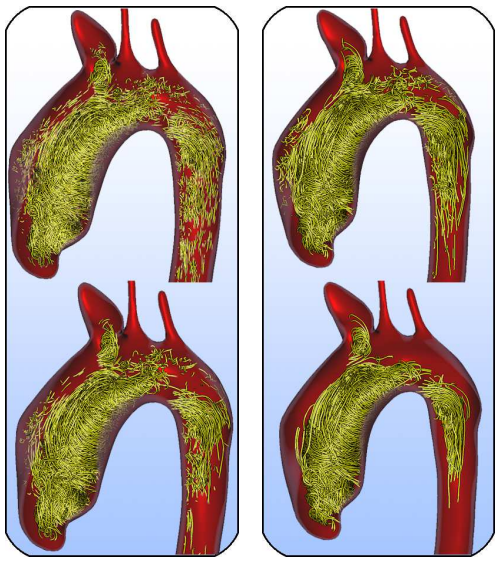

(a) (b)

Fig. 3: Influence of smoothing predicates and postprocessing.
(a) Thresholding the calculated vortex criterion without (top) and with (bottom) previously applied smoothing. (b) Comparison of a result without (top) and with (bottom) postprocessing using the bending energy predicate.

5.3 Comparison of Local Vortex Criteria

Based on the previous procedure, we investigate, which local vortex criterion provides pathlines that reliably describe vortex structures in 4D PC-MRI data. We consider the λ_2- and Q-criterion, reduced velocity, cores of swirling particle motion (COSPM), vorticity, torsion and normalized helicity (recall Sec. 2).
We applied our procedure to ten datasets. Since the results are consistent, for sake of simplicity, we demonstrate the comparison for one representative case, shown in Figure 4. The patient has an ectasia in the ascending aorta. The manual exploration revealed three vortices: one large vortex in the ascending aorta that is present during the complete heart cycle and two smaller ones in the distal aortic arch that occur only during the systole.

5.3.1 Definition of Quality Criteria

A quantitative comparison will be challenging due to the missing ground truth. Thus, we rely on subjective impressions and formulate key questions for the vortex criteria in cooperation with domain experts (e.g. radiologists and cardiologists). They put great emphasis on the correctness of the results and the capability of our procedure to extract and present different vortex types with expressive pathlines. We complemented their expectations with considerations about the vortex criterias' value domains and the possibility to use universal thresholds. In summary, we performed the evaluation considering the following key aspects:

Fixed Minimum and Maximum: Is there a fixed minimum and/or maximum of the calculated value domain? This facilitates the identification of a general applicable threshold for all datasets.

Implicit Threshold: Is there an implicit threshold to distinguish between vortex and non-vortex regions? This would make the previous question superfluous.

Constant Vortex Core Values: Are the values of the criterion constant along vortex cores? This aspect influences the filtering behavior. If the values are constant, vortices are filtered from the outside to the inside when the threshold is increased.

Correctness: Is our extraction procedure able to find at least every vortex that was discovered by the physicians' previously performed manual exploration of the datasets?

Helical and Vortical Flow: Vortices can be classified according to their appearance: swirling pathlines with a strong movement along the vortex core are helical, whereas pathlines that tend to swirl in the plane are vortical. Is the employed vortex criterion able to determine both?

Vortex Shape: Is the shape of a vortex pointed out sufficiently? Its swirling characteristic should be comprehensibly presented by the pathlines.

Pathline Quality: The extracted vortices should be presented by pathlines with long and continuous courses. False-positive results as well as short pathline fragments are unwanted.

All thresholds were manually adjusted at this point to achieve the best possible findings. In addition, we decided not to use the bending energy line predicate 3 for postprocessing in order to emphasize the actual differences between the results.

5.3.2 Observations

In the following, we describe the main outcomes of the discussion with the domain experts about the results of each vortex criterion. Our key questions are also answered in short in Figure 4a to 4g. A green check or red cross answers yes/no questions and a green, yellow or red bar stands for a good, medium or bad rating of a property. Figure 4h is an anticipation of a result achieved with our final procedure described in 5.3.3 and provided as a reference. For that reason, this is the only result with applied postprocessing.

Vorticity: The vorticity criterion (see Fig. 4a) preserves pathlines in helical and vortical regions, but exhibits a high false-positive rate especially near the vessel boundaries. The quality of the pathlines is appropriate. There is a fix minimum value of 0, but the maximum depends directly on the derivatives of the occurring velocities. Thus, there is no fixed peak value among different vortices. The same yields for a general threshold. A small vortex often vanishes before the shape of a larger one is pointed out sufficiently. This can even happen within a single vortex since the criterion is not constant along vortex cores or within vortex regions.

Torsion: By using the torsion (see Fig. 4b) it is hardly possible to extract pathlines that meet our expectations. Though the pathline density is higher in vortex regions, they are highly fragmented. Not all vortices are captured correctly and a large amount of false-positive pathlines is present. Helical flow is extracted rather than vortical flow since the torsion describes the twisting of a curve out of the plane. The minimum of 0 and maximum of 1 are fixed values, but we could not determine a generally applicable threshold.

Normalized Helicity: The results of the normalized helicity (see Fig. 4c) are very similar to the ones achieved by using the torsion. Especially vortex flow is extracted insufficiently. A unique characteristic of the helicity is its sign that helps to characterize the orientation of a vortex into left- and right-handed. The value domain ranges from -1 to $+1$, where 0 is no helicity and the absolute of 1 is the maximum left- or right-handed swirling strength.

Reduced Velocity: The reduced velocity (see Fig. 4d) is a projection of the velocity vector onto a plane orthogonal to the vortex core direction. If the angle between the velocity vector and the vortex core direction is small, the length of the projected vector, the reduced velocity, is 0. This minimum value is constant along the vortex cores of all vortices. Applying a threshold results in progressively removing off the pathlines from the outer regions to the vortex core. This is suitable for cases where the pathlines swirl helically along the vortex core direction. Pathlines that represent vortical flow tend to swirl in a plane with increasing distance. These pathlines are filtered away early when increasing the threshold and, consequently, the extracted vortices may appear thinly. In addition, this problem can lead to the unwanted interruptions of pathlines. Also, smaller regions of vortical flow are not always captured correctly. An implicit threshold is not given for the reduced velocity, but reasonable values should be close to 0.

Cores of Swirling Particle Motion: COSPM (see Fig. 4e) is the extension of the reduced velocity from steady to unsteady 3D flow. The results are very similar, which is an indication that the flow alteration over time is rather small in the cardiac 4D PC-MRI datasets. This fact increases the reliability of steady flow vortex criteria applied to the unsteady blood flow. The minimum of 0 and maximum of 1 are fixed values. As before, a value of 0 means that a position is directly on the vortex core.

Q-Criterion: The Q-criterion (see Fig. 4f) was able to extract every single vortex in our datasets. The pathline quality meets our requirements and there is an implicit threshold of $Q > 0$. The criterion is neither constant along the vortex core nor has a behavior like the reduced velocity or COSPM regarding the distance to the vortex core. Therefore, increasing the threshold should be avoided, since it cannot be reliably predicted which pathlines will be maintained or filtered.

λ_2-Criterion: Like the Q-criterion, the λ_2-criterion (see Fig. 4g) was able to detect every vortex in our datasets. Their results are nearly identical. Using the λ_2-criterion made it likewise possible to extract all vortices correctly with the same pathline quality. The only difference to the Q-criterion is that 0 is the maximum value and the implicit threshold is given by $\lambda_2 < 0$.

5.3.3 Summary

Based on the previous comparison, the λ_2- and Q-criterion have shown the best results. In accordance with the domain experts, we cannot see a significant difference and recommend the usage of both criteria

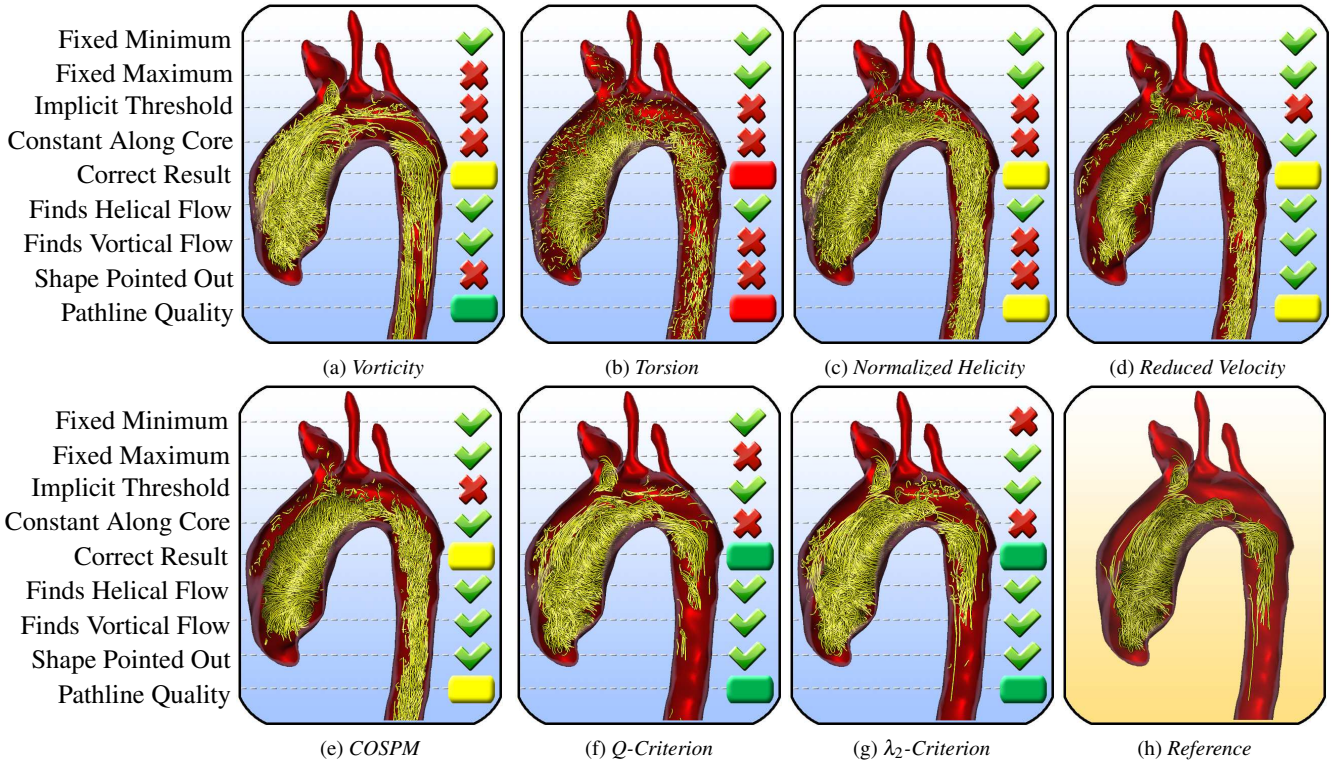

(a) *Vorticity* (b) *Torsion* (c) *Normalized Helicity* (d) *Reduced Velocity*

(e) *COSPM* (f) *Q-Criterion* (g) λ_2*-Criterion* (h) *Reference*

Fig. 4: *The images from (a) to (g) show results using our vortex extraction procedure combined with different local vortex criteria. The properties on the left refer to the questions in Section 5.3. They are answered in each image either with yes (green check), no (red cross) or scored with bad (red), medium (yellow) or good (green). Thresholds were adjusted manually and we went without postprocessing at this point. (h) shows a result extracted with our final procedure, λ_2 with postprocessing*, as a reference.

for the extraction of vortices in blood flow. For detailed differences between the λ_2- and the Q-criterion we refer to Sahner et al. [34].
A possible explanation for their robust results is that in contrast to all other criteria, λ_2 and Q solely analyze the derivatives of the velocity vectors (the Jacobian matrix). The reduced velocity, for instance, uses the Jacobian matrix *and* the velocity vectors. This might amplify noise in the data and introduce further errors.
We found that the λ_2-criterion is more established among blood flow-specific works [4, 36, 39] and decided to use it as well. The necessary eigenvalue analysis of the Jacobian matrix is done on the GPU using Cardano's method [21].
The implicit threshold of $\lambda_2 < 0$ will be used for the first vortex line predicate. For the second (mean) vortex predicate, we recommend the removal of points representing the lower 10% of the value margin. Postprocessing via the bending energy predicate carries the risk of removing short pathlines representing very small vortices, especially when other comparatively large vortices exist. Therefore, we suggest to rely on the user's judgment and offer this last step as optional manual postprocessing.
Since we did not find any vortex that was exclusively detected by another vortex criterion and not by λ_2, we decided not to combine different vortex criteria.
In summary, our final procedure is to integrate about 30,000 uniformly distributed pathlines and then calculate the characteristic set $\mathbb{C}_{\text{vortex}}$ as:

$$\begin{aligned} \mathbb{C}_{\text{vortex}} &= P_{\sigma,25}(P_{\mathbb{V}}^{\lambda_2}),\ \hat{p} < 0 \\ &\rightarrow P_{\oslash}(P_{\mathbb{V}}^{\lambda_2}),\ \underline{90\%} \\ &\rightarrow P_{\Gamma}^{\text{bendingEnergy}},\ t_{\text{manual}} \end{aligned} \tag{7}$$

The successive vortex extraction is illustrated in Figure 2c and a result for the same dataset is shown in Figure 4h. On the average taken over all datasets, the mean pathline length, measured after application of the first and last line predicate, becomes three times larger. This supports the claim that pathlines of increased quality are obtained.

Excluding the preprocessing (recall Sec. 3.2), the only necessary user interaction is to adjust the bending energy threshold for postprocessing. Furthermore, if the aforementioned standard parameters are not used, the required input extends to choosing the number of seed points as well as adjusting three successive thresholds.

6 Results and Informal Evaluation

We applied our vortex extraction method to ten 4D PC-MRI datasets of the aorta and pulmonary artery. In the following, we describe two clinical cases in detail and then give an overview of the other ones. We showed results of our extraction procedure to one cardiologist as well as two radiologists and asked them to relate occurring vortex patterns to the present pathologies. The evaluation was performed informally and the domain experts were not required to solve tasks.
The integration of $30,000$ pathlines and calculation of the λ_2-criterion is performed in less than 10ms on a GeForce GTX 680. The data transfer between GPU and CPU takes another 1.7s.
The presented images are directly captured from the animation. In addition to the static pathline visualization, freely scalable arrowheads are added at positions, where a pathline's time matches the animation time, to make the current flow directions easier recognizable.

6.1 Tetralogy of Fallot with Pulmonic Regurgitation

The first case has a Tetralogy of Fallot. A VSD surgery has been performed in the past. The patient mentions a fast exhaustion with dyspnea during physical activities, nausea, a pulling pain into the legs and regularly occurring palpitations.
Ultrasonography revealed the existence of distinct diastolic retrograde flow in the pulmonary artery. A closer examination of the heart showed a mild hypertrophy of the right ventricle, although a significant narrowing of the pulmonary artery was not present. According to the admission note, the regurgitation fraction, which is the ratio of retrograde and antegrade flow, is about 2% from the aorta back into the left ventricle and about 30% from the pulmonary artery back into the right

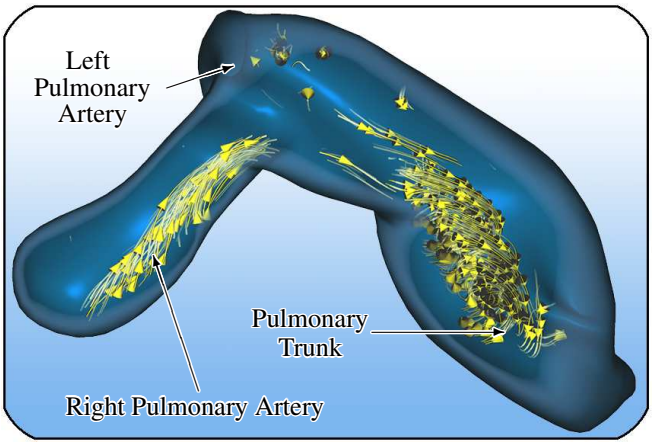

Fig. 5: *The pulmonary artery of a Tetralogy of Fallot patient. About 30% of the blood flows back into the right ventricle during the diastole due to an improperly closing valve. This percentage is high enough to specify the circumstances as pulmonary insufficiency. Vortices are present in the right pulmonary artery and the pulmonary trunk close to the valve.*

ventricle. The latter characterizes a severe pulmonary insufficiency. The hypertrophic right ventricle may be encouraged by the increased blood pressure due to the pulmonary regurgitation.

For clinical research, a 4D PC-MRI measurement was performed. The qualitative analysis of the complete flow in the pulmonary artery shows a clearly visible retrograde flow even without the enhancement of certain data aspects or features. Diastolic high velocity flow near both the aortic and pulmonary valve could be observed. In either case, a vortex is present during the diastole, shown in Figure 1 and Figure 5, respectively. The vortices occur when the blood flows back into the ventricles through a small gap caused by improperly closing valves.

Our quantification results verify the regurgitation fractions of 30% and 2%. Clearly, the situation in the pulmonary artery is pathologic and explains the vortex near the valve. This small percentage of physiological retrograde flow seems to be sufficient to cause the vortex near the aortic valve. Thus, the existence of such a vortex should not be seen as evidence for pathologic retrograde flow, but rather lead to further investigations.

All necessary information and explanations of the symptoms for the case are present in this dataset and our domain experts were able to diagnose the same pathology in the pulmonary artery.

6.2 Aneurysm and BAV with former Coarctation

The primary disease of the second case was a coarctation, which was widened via balloon dilatation. Based on a suspicion for a re-coarctation nine years later, a new examination was performed combined with the acquisition of a 4D PC-MRI dataset. The patient has no physical limitations. Only minor symptoms like a casually occurring tingling in the left arm are present.

The re-coarctation could be excluded by doing a cardiac catheterization. An MRI of the heart showed a large aneurysm in the left subclavian artery and an ectatic distal aortic arch. The aneurysm in an early stage was already known from the first examination, but has grown progressively since then.

The first look at the overall flow revealed a huge vortex during the full systole and diastole ranging from the dilated left subclavian artery to the descending aorta, illustrated in Figure 6 during the systole (left) and diastole (right). Our vortex extraction procedure reveals no pathological findings in the pulmonary artery, but an abnormal vortex structure near the aortic valve during systole. Hope et al. [15] found swirling flow in the ascending aorta during the systole in 75% of their BAV cases and only in 6% of the healthy individuals with tricuspid aortic valves. Considering these results, it is likely that the BAV causes this vortex in our dataset as well. This assumption, however, could not

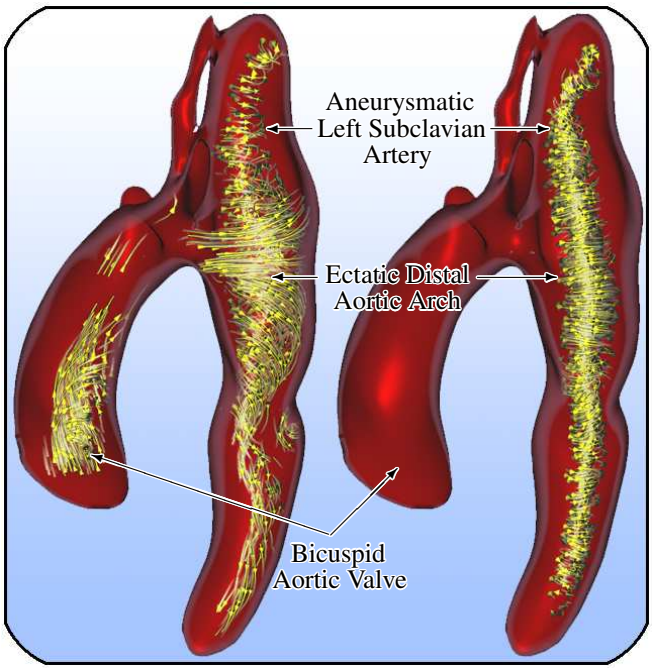

Fig. 6: *Aorta of a patient with an aneurysmatic left subclavian artery and a dilated distal aortic arch. A huge vortex is present during the full systole (left) and diastole (right). The systolic vortex in the ascending aorta could be caused by the patient's bicuspid aortic valve.*

be confirmed with certainty by the domain experts, but such a flow behavior could indicate a valve defect and lead to further investigations.

Further discussions about the aneurysmatic left subclavian artery revealed another important flow behavior: blood passes the area of the former coarctation and then, due to the altered vessel shape, keeps flowing straight ahead instead of following the distal aortic arch leading into the descending aorta. The flow impinges on the surface and then starts swirling upwards into the subclavian artery and downwards along the descending aorta. Recent works observed an increased wall shear stress in regions where high velocity flow impinges on the vessel's surface. They agree that abnormally high wall shear stress is one main cause for the initial development of aneurysms [30, 37]. As a consequence, the permanent stress caused by the swirling flow could be one important factor for the patient's progressively dilating vessel.

Again, the 4D PC-MRI data complemented the diagnosis information, helped to explain the symptoms and supported the understanding of the case. The aneurysmatic subclavian artery as well as the ectatic distal aortic arch could be determined easily and the systolic vortex near the aortic valve gave a clear hint towards the BAV. In addition, we think that the altered vessel geometry is only assessable by evaluating the flow and its excessive swirling behavior.

6.3 Overview of other Cases

Figure 7a shows the patient we presented previously for the vortex criteria comparison. The large vortex in the ascending aorta keeps swirling during the diastole and flows back through the aortic valve into the left ventricle. Further quantification shows a pathologic regurgitation fraction of about 15-20%. According to our experts, this fact can support the decision whether or not to implant an artificial valve.

The patient shown in Figure 7b has a coarcation and a slightly dilated ascending aorta. A small vortex is observable in the aortic arch where the narrowing is. Analogous to all our other datasets with dilated ascending aortas, a large vortex is present in this part of the vessel.

A similar case is shown in Figure 7c and Figure 7d. The patient has an ectatic ascending aorta and one large vortex is present during the systole (see Fig. 7c). In contrast to the first example, the vortex disappears in the diastole and no significant retrograde flow is determinable. The pulmonary artery shows a slight vortex in the pulmonary trunk near the valve during the systole (see Fig. 7d). Considering the results re-

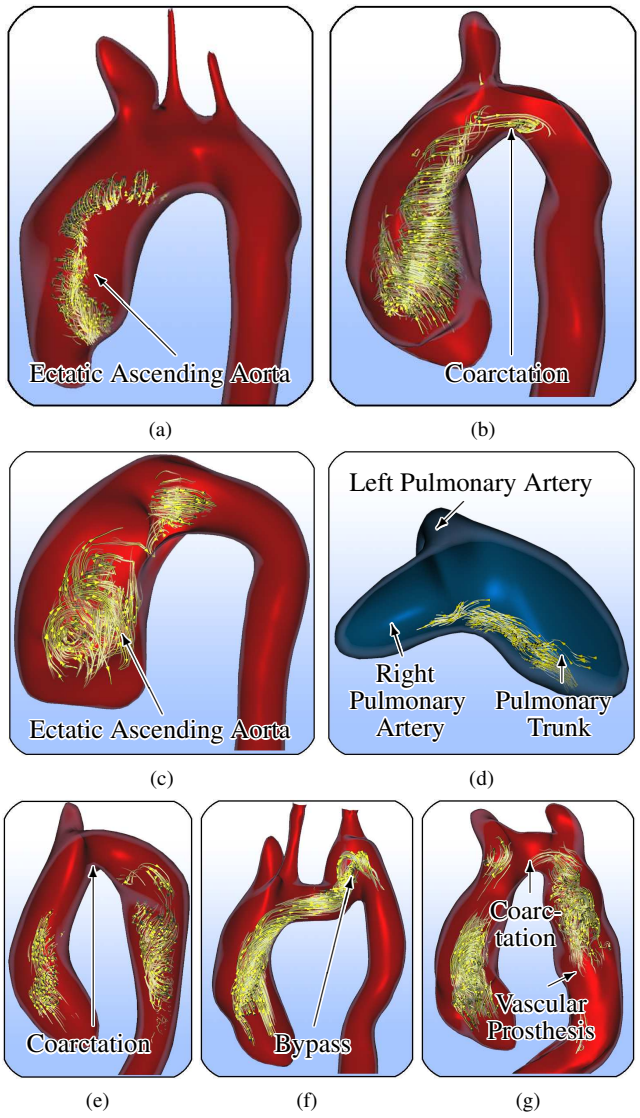

Fig. 7: *(a) Patient with an ectasia in the ascending aorta. Two smaller vortices are present in the aortic arch during the systole. The large one in the ascending aorta keeps swirling during the whole diastole as well and flows back into the left ventricle. The regurgitation fraction is pathologic with about* 15 *to* 20%. *(b) A small vortex occurs in the aortic arch of this patient with a coarctation. The slightly dilated ascending aorta shows a large vortex during the systole. (c, d) The patient has an ectatic ascending aorta. (c) A large vortex is present during the systole that vanishes in the diastole. (d) A systolic vortex near the pulmonary valve could indicate a bicuspidality. (e) Patient with a coarctation. Besides a vortex in the ascending aorta, there is one after the narrowed region that is probably evolved by the altered vessel geometry. All vortices occur in the systole. (f) Patient with a bypass. The altered vessel geometry promotes the formation of a large helix during the systole. (g) Patient with a coarctation and a vascular prosthesis. Three vortices are present during the systole. One is close to the valve and could indicate a defect. A second small vortex is observable in the aortic arch. The third large one occurs in the region of the prosthesis and is likely caused by the anomalous vessel shape.*

garding aortic valve defects, this could indicate a bicuspid pulmonary valve. Assuming that vortex flow promotes the development of vessel dilations and, in turn, bicuspid valves encourage vortex flow, the conclusion could be drawn that bicuspidalities increase the risk of an ectasia development.

Figure 7e shows a patient with a coarctation. The narrowed vessel geometry seems to cause the vortex from the distal aortic arch into the descending aorta. Again, we can observe a vortex in the ascending aorta during the systole that could indicate a BAV.

The case shown in Figure 7f had undergone a bypass operation. There is one large helix present during the systole that is likely promoted by the altered course of the vessel.

The last example in Figure 7g shows a similar case. The patient has a coarctation and a vascular prosthesis implant. The occurring vortex patterns are comparable to the ones in Figure 7e and were possibly caused by the same reasons. An additional small vortex is present in the aortic arch. All vortices occur in the systole.

Our two healthy volunteers were, as expected, without pathologic findings. The same yields for the pulmonary arteries of all cases except for the two we showed in Figure 7d and Figure 5.

7 Conclusion and Future Work

We have shown that our approach reliably extracts vortices in the aorta and pulmonary artery based on 4D PC-MRI measured flow information. We considered a result as correct if at least all vortices were extracted that experts were able to discover manually. The extraction achieves real-time capability due to its entire computation on the GPU. The novelty of our approach consists of a detailed investigation of several vortex criteria. We identified λ_2 as the most appropriate local vortex criterion for cardiac 4D PC-MRI datasets, yet the limited diversity of our datasets might alleviate the generality of this result. We incorporate line predicates to extract meaningful pathlines, which describe vortex flow structures. Their quality is high and meets the domain experts' and our requirements. The experts came to similar conclusions regarding the relation of present pathologies and occurring vortices for the presented cases. Thus, the straight forward and semi-automatic extraction pipeline in combination with reasonable default parameters ensures the ease of use of our method and minimizes the inter-observer variability.

The results allow a more precise diagnosis, support treatment decisions, and facilitate the understanding of the progression of cardiovascular diseases like ectasias and aneurysms. Vortices are a strong indicator for certain pathologies of the cardiovascular system and complement other features like velocities, flow rates and the amount of retrograde flow. However, the correlation between pathologies and vortex flow patterns is an ongoing research topic. Our clinical collaborators indicate that with more confidence in our tools, they may replace the standard 2D blood flow measurements in the future. This would be a big step forward, since 4D blood flow measurements would leave the stage of an experimental modality only used for selected cases. An important requirement for future work will be to optimize the workflow and usability of tools.

For the correct assessment of the clinical relevance of cardiac blood flow, the state of the vessel wall is essential. On the one hand, the movement, especially for large vessels, should be taken into account. This requires a reliable spatio-temporal segmentation. On the other hand, such a segmentation would enable a reliable determination of the wall shear stress (WSS). According to Potters et al. [33], the effect of false segmentations, especially concerning the vessel diameter, was substantial on the calculated vectorial WSS in their experiments with phantoms. The relation of the WSS to different combinations of vortices and pathologies could help to better understand the development of certain diseases like ectasias and aneurysms.

The line predicate technique is flexible enough to be extended, so that more flow characteristics can be determined (see Born et al. [4]). Possible targets are laminar flow, high velocity flow during the diastole, the separation of antegrade and retrograde flow, flow that impinges on the vessel walls with high velocities and flow that causes high WSS.

A reliable and automatic classification of different vortex types could provide additional help in understanding the relation between vortex patterns and different pathologies.

Acknowledgments

We would like to thank Anja Hennemuth for fruitful discussions and making the MeVisFlow software available to us.

REFERENCES

[1] J. Benedik, K. Pilarczyk, D. Wendt, J. Indruch, R. Flek, K. Tsagakis, S. Alaeddine, and H. Jakob. Ascending Aortic Wall Cohesion: Comparison of Bicuspid and Tricuspid Valves. *Cardiol Res Pract*, 2012:180238, 2012.

[2] H. G. Bogren, M. H. Buonocore, and R. J. Valente. Four-Dimensional Magnetic Resonance Velocity Mapping of Blood Flow Patterns in the Aorta in Patients with Atherosclerotic Coronary Artery Disease compared to Age-Matched Normal Subjects. *J Magn Reson Imag*, 19(4):417 – 427, 2004.

[3] S. Born, M. Markl, M. Gutberlet, and G. Scheuermann. Illustrative Visualization of Cardiac and Aortic Blood Flow from 4D MRI Data. In *Pacific Vis*, 2013. (to appear).

[4] S. Born, M. Pfeifle, M. Markl, M. Gutberlet, and G. Scheuermann. Visual Analysis of Cardiac 4D MRI Blood Flow Using Line Predicates. *IEEE TVCG*, 19:900 – 912, 2013.

[5] J. R. Cebral, F. Mut, J. Weir, and C. M. Putman. Association of Hemodynamic Characteristics and Cerebral Aneurysm Rupture. *Am J Neurorad*, 32(2):264 – 270, 2011.

[6] C. Dìaz and L. A. Robles. Fast Noncontinuous Path Phase-Unwrapping Algorithm based on Gradients and Mask. In *CIARP*, volume 3287 of *Lecture Notes in Computer Science*, pages 116 – 123, 2004.

[7] J. R. Dormand and P. J. Prince. A Family of Embedded Runge-Kutta Formulae. *J Comput Appl Math*, 6:19 – 26, 1980.

[8] C. Francois, S. Srinivasan, M. Schiebler, S. Reeder, E. Niespodzany, B. Landgraf, O. Wieben, and A. Frydrychowicz. 4D Cardiovascular Magnetic Resonance Velocity Mapping of Alterations of Right Heart Flow Patterns and Main Pulmonary Artery Hemodynamics in Tetralogy of Fallot. *J Cardiovasc Magn Reson*, 14(1):16, 2012.

[9] R. Gasteiger, M. Neugebauer, O. Beuing, and B. Preim. The FLOWLENS: A Focus-and-Context Visualization Approach for Exploration of Blood Flow in Cerebral Aneurysms. *IEEE TVCG*, 17(12):2183 – 2192, 2011.

[10] R. Gasteiger, M. Neugebauer, C. Kubisch, and B. Preim. Adapted Surface Visualization of Cerebral Aneurysms with Embedded Blood Flow Information. In *Proc EG VCBM*, pages 25 – 32, 2010.

[11] J. Geiger, M. Markl, L. Herzer, D. Hirtler, F. Loeffelbein, B. Stiller, M. Langer, and R. Arnold. Aortic Flow Patterns in Patients with Marfan Syndrome assessed by Flow-Sensitive Four-Dimensional MRI. *J Magn Reson Imag*, 35(3):594 – 600, 2012.

[12] M. Grothoff, B. Spors, H. Abdul-Khaliq, M. Abd El Rahman, V. Alexi-Meskishvili, P. Lange, R. Felix, and M. Gutberlet. Pulmonary Regurgitation is a Powerful Factor Influencing QRS Duration in Patients After Surgical Repair of Tetralogy of Fallot. A Magnetic Resonance Imaging (MRI) Study. *Clin Res Cardiol*, 95(12):643 – 649, 2006.

[13] M. Grothoff, B. Spors, H. Abdul-Khaliq, and M. Gutberlet. Evaluation of Postoperative Pulmonary Regurgitation after Surgical Repair of Tetralogy of Fallot: Comparison between Doppler Echocardiography and MR Velocity Mapping. *Pediatr Radiol*, 38(2):186 – 191, 2008.

[14] A. Hennemuth, O. Friman, C. Schumann, J. Bock, J. Drexl, M. Huellebrand, M. Markl, and H.-O. Peitgen. Fast Interactive Exploration of 4D MRI Flow Data. *SPIE Proc*, 7964, 2011.

[15] M. D. Hope, J. Wrenn, M. Sigovan, E. Foster, E. E. Tseng, and D. Saloner. Imaging Biomarkers of Aortic Disease - Increased Growth Rates with Eccentric Systolic Flow. *J Amer Coll Cardiol*, 60(4):356 – 357, 2012.

[16] H. Hoppe. New Quadric Metric for Simplifying Meshes with Appearance Attributes. In *10th IEEE Vis Proc*, pages 59 – 66, 1999.

[17] M. Hummel, C. Garth, B. Hamann, H. Hagen, and K. Joy. IRIS: Illustrative Rendering for Integral Surfaces. *IEEE TVCG*, 16(6):1319 – 1328, 2010.

[18] J. Hunt. Vorticity and Vortex Dynamics in Complex Turbulent Flows. *Trans Can Soc Mech Eng*, 11:21 – 35, 1987.

[19] J. Jeong and F. Hussain. On the Identification of a Vortex. *J Fluid Mech*, 285:69 – 94, 1995.

[20] C. Koehler, T. Wischgoll, H. Dong, and Z. Gaston. Vortex Visualization in Ultra Low Reynolds Number Insect Flight. *IEEE TVCG*, 17(12):2071 – 2079, 2011.

[21] J. Kopp. Efficient Numerical Diagonalization of Hermitian 3x3 Matrices. *Int J Mod Phys C*, 19(3):523 – 548, 2008.

[22] J.-W. Lankhaar, M. B. M. Hofman, J. T. Marcus, J. J. M. Zwanenburg, T. J. C. Faes, and A. Vonk-Noordegraaf. Correction of Phase Offset Errors in Main Pulmonary Artery Flow Quantification. *J Magn Reson Imag*, 22(1):73 – 79, 2005.

[23] Y. Levy, D. Degani, and A. Seginer. Graphical Visualization of Vortical Flows by means of Helicity. *Am Inst Aeronaut Astronaut J*, 28:1347 – 1352, 1990.

[24] J. Lotz, C. Meier, A. Leppert, and M. Galanski. Cardiovascular Flow Measurement with Phase-Contrast MR Imaging: Basic Facts and Implementation. *Radiographics*, 22(3):651 – 671, 2002.

[25] M. Markl, A. Frydrychowicz, S. Kozerke, M. D. Hope, and O. Wieben. 4D Flow MRI. *J Magn Reson Imag*, 36(5):1015 – 1036, 2012.

[26] T. McLoughlin, R. S. Laramee, R. Peikert, F. H. Post, and M. Chen. Over Two Decades of Integration-Based, Geometric Flow. *Comp Graph Forum*, 29(6):1807 – 1829, 2010.

[27] S. Mendis, P. Puska, and B. Norrving. *Global Atlas on Cardiovascular Disease Prevention and Control*. World Health Organization, World Heart Federation and World Stroke Organization, 2011.

[28] M. Neugebauer, R. Gasteiger, O. Beuing, V. Diehl, M. Skalej, and B. Preim. Map Displays for the Analysis of Scalar Data on Cerebral Aneurysm Surfaces. 28 (3):895 – 902, 2009.

[29] M. Neugebauer, G. Janiga, O. Beuing, M. Skalej, and B. Preim. Anatomy-Guided Multi-Level Exploration of Blood Flow in Cerebral Aneurysms. *Comp Graph Forum*, 30(3):1041 – 1050, 2011.

[30] A. M. Nixon, M. Gunel, and B. E. Sumpio. The Critical Role of Hemodynamics in the Development of Cerebral Vascular Disease. *J Neurosurg*, 112(6):1240 – 1253, 2010.

[31] R. Peikert and M. Roth. The "Parallel Vectors" Operator – A Vector Field Visualization Primitive. In *10th IEEE Vis Proc*, pages 263 – 270, 1999.

[32] A. Pobitzer, A. Lez, K. Matkovic, and H. Hauser. A Statistics-Based Dimension Reduction of the Space of Path Line Attributes for Interactive Visual Flow Analysis. In *Pacific Vis*, pages 113 – 120, 2012.

[33] W. V. Potters, P. van Ooij, E. Vanbavel, and A. Nederveen. Vectorial Wall Shear Stress Calculations in Vessel Structures using 4D PC-MRI. *J Cardiovasc Magn Reson*, 14(1):W5, 2012.

[34] J. Sahner, T. Weinkauf, and H.-C. Hege. Galilean Invariant Extraction and Iconic Representation of Vortex Core Lines. In *Proc Joint Eurograph / IEEE VGTC*, pages 151 – 160, 2005.

[35] T. Salzbrunn, C. Garth, G. Scheuermann, and J. Meyer. Pathline Predicates and Unsteady Flow Structures. *The Visual Computer*, 24(12):1039 – 1051, 2008.

[36] T. Schafhitzel, J. E. Vollrath, J. P. Gois, D. Weiskopf, A. Castelo, and T. Ertl. Topology-Preserving λ_2-Based Vortex Core Line Detection for Flow Visualization. *Comp Graph Forum*, 27(3):1023 – 1030, 2008.

[37] D. M. Sforza, C. M. Putman, and J. R. Cebral. Hemodynamics of Cerebral Aneurysms. *Annu Rev Fluid Mech*, 41(1):91 – 107, 2009.

[38] K. Shi, H. Theisel, H. Hauser, T. Weinkauf, K. Matkovic, H.-C. Hege, and H.-P. Seidel. Path Line Attributes - an Information Visualization Approach to Analyzing the Dynamic Behavior of 3D Time-Dependent Flow Fields. In *Topology-Based Methods in Visualization II*. 2009.

[39] A. F. Stalder, A. Frydrychowicz, A. Harloff, Q. Yang, J. Bock, J. Hennig, K. C. Li, and M. Markl. Vortex Core Detection and Visualization using 4D Flow-Sensitive MRI. In *18th Int Scien Meet Proc*, 2010.

[40] D. Sujudi and R. Haimes. Identification Of Swirling Flow In 3D Vector Fields. *J Fluid Mech*, 5:69 – 94, 1995.

[41] G. Taubin, T. Zhang, and G. Golub. Optimal Surface Smoothing as Filter Design. In *Comp Vis - ECCV '96*, volume 1064 of *Lecture Notes in Computer Science*, pages 283 – 292. 1996.

[42] H. Theisel, T. Weinkauf, H.-C. Hege, and H.-P. Seidel. Stream Line and Path Line Oriented Topology for 2D Time-Dependent Vector Fields. In *15th IEEE Vis Proc*, pages 321 – 328, 2004.

[43] R. van Pelt, J. O. Bescos, M. Breeuwer, R. E. C., M. E. Gröller, B. ter Haar Romenij, and A. Vilanova. Exploration of 4D MRI Blood Flow using Stylistic Visualization. *IEEE TVCG*, 16(6):1339 – 1347, 2010.

[44] S. Venkataraman. 4D Visualization of Cardiac Flow. Nvidia GTC 2010 Talk.

[45] T. Weinkauf, J. Sahner, H. Theisel, and H.-C. Hege. Cores of Swirling Particle Motion in Unsteady Flows. *IEEE TVCG*, 13(6):1759 – 1766, 2007.